Sains Malaysiana 51(9)(2022): 2857-2871
http://doi.org/10.17576/jsm-2022-5109-10

Metal and Metal Oxide Nanoparticles from *Mimusops elengi* Linn. Extract: Green Synthesis, Antioxidant Activity, and Cytotoxicity

(Nanozarah Logam dan Oksida Logam daripada *Mimusops elengi* Linn. Ekstrak: Sintesis Hijau, Aktiviti Antioksidan dan Kesitotoksikan)

SELLY ARVINDA RAKHMAN, TANYARATH UTAIPAN, CHAROEN PAKHATHIRATHIEN & WEERAYA KHUMMUENG*

Department of Science, Faculty of Science and Technology, Prince of Songkla University, Pattani, 94000, Thailand

Received: 16 December 2021/Accepted: 30 March 2022

ABSTRACT

In this study, both silver (Ag) and zinc oxide (ZnO) nanoparticles are green synthesized using a water extract of the *Mimusops elengi* Linn. leaf. The methods are simple, inexpensive, nontoxic, and eco-friendly. The AgNPs and ZnONPs are formed using phytochemical substances in *M. elengi* leaf extract at room temperature. The phenolics and flavonoids in the leaf extract is the key compounds that act as the metal-reducing agents. The effective parameters of the green synthesis (the metal concentration, leaf extract concentration, pH, temperature, and reaction time) are evaluated. The formation of the metal and metal oxide nanoparticles (NPs) are confirmed through colour change visuals, ultraviolet–visible (UV-vis) spectroscopy (UV-vis), and Fourier transform infrared (FTIR) spectroscopy. The morphological and crystalline characterizations of the NPs are established using transmission electron microscopy (TEM) and X-ray diffraction (XRD). The TEM results indicated that the AgNPs are predominantly spherical in shape with an average particle size of 22.12 nm. The ZnONPs have mostly rod-like morphology with an average size of 28.44 nm. The antioxidant activity and cytotoxicity of the synthesized NPs against colon cancer cells (Caco-2 cells) are evaluated; the obtained NPs exhibited good free radical scavenging activity through DPPH, ABTS, and FRAP assays. The cytotoxicity results demonstrated that only the 2,000-ppm extract had any potential against the Caco-2 cells; both the AgNPs and ZnONPs had no effect on Caco-2 cells. However, regarding human health, metal NPs are safe to use and are useful in the other applications.

Keywords: Antioxidant; cytotoxicity; green synthesis; *Mimusops elengi* Linn; nanoparticles

ABSTRAK

Dalam kajian ini, kedua-dua nanozarah perak (Ag) dan zink oksida (ZnO) disintesis secara hijau menggunakan ekstrak air daun *Mimusops elengi* Linn. Kaedahnya mudah, murah, tidak toksik dan mesra alam. AgNPs dan ZnONPs dibentuk menggunakan bahan fitokimia dalam ekstrak daun *M. elengi* pada suhu bilik. Fenol dan flavonoid dalam ekstrak daun adalah sebatian utama yang bertindak sebagai agen pengurangan logam. Parameter berkesan sintesis hijau (kepekatan logam, kepekatan ekstrak daun, pH, suhu, dan masa tindak balas) dinilai. Pembentukan nanozarah logam dan logam oksida (NPs) disahkan melalui visual perubahan warna, spektroskopi tampak ultraungu (UV-vis) (UV-vis) dan spektroskopi inframerah transformasi Fourier (FTIR). Pencirian morfologi dan hablur NP menggunakan mikroskop elektron penghantaran (TEM) dan pembelauan sinar-X (XRD). Keputusan TEM menunjukkan bahawa AgNPs kebanyakannya berbentuk sfera dengan saiz zarah purata 22.12 nm. ZnONPs kebanyakannya mempunyai morfologi seperti batang dengan saiz purata 28.44 nm. Aktiviti antioksidan dan kesitotoksikan NP yang disintesis terhadap sel kanser kolon (sel Caco-2) dinilai; NP yang diperoleh mempamerkan aktiviti penghapusan radikal bebas yang baik melalui ujian DPPH, ABTS dan FRAP. Keputusan kesitotoksikan menunjukkan bahawa hanya ekstrak 2,000-ppm mempunyai potensi terhadap sel Caco-2; kedua-dua AgNP dan ZnONP tidak mempunyai kesan ke atas sel Caco-2. Walau bagaimanapun, mengenai kesihatan manusia, NP logam selamat digunakan dan berguna dalam aplikasi lain.

Kata kunci: Antioksidan; kesitotoksikan; *Mimusops elengi* Linn; nanozarah; sintesis hijau

Introduction

Nanoparticles (NPs) or ultrafine particles fundamentally refer to particles with a diameter ranging from 1 to 100 nm (Khan et al. 2019). These particles receive considerable scientific attention due to their unique features such as high surface area-to-volume ratios and interface-dominated structures that make them quite useful in a wide variety of applications (Istiqola & Syafiuddin 2020; Mondéjar-López et al. 2021). In addition, both the elemental metal NPs (e.g., Ag, Au, Fe, and Cu) and metal oxide NPs (e.g., ZnO, FeO, SiO_2, and TiO_2) are heavily researched. The metal oxide NPs receive substantial attention due to their preferable photocatalytic properties (Bandeira et al. 2020; Dubey et al. 2015). Among the metallic NPs, silver NPs (AgNPs) are vastly utilized in different application areas. In the pharmaceutical industry, AgNPs are vital in the manufacturing of skin ointments and creams for burns and wound infections (Paladini & Pollini 2019). In the food industry, AgNPs are the most commonly used antimicrobial substance (Kokila et al. 2016). AgNPs act as a source of the Ag^+ ion that typically bonds to membrane proteins to accelerate the generation of reactive oxygen species (ROS) that cause death in bacterial cells due to oxidative stress (Ahmed et al. 2018). Zinc oxide NPs (ZnONPs), which are metal oxide NPs, are predominantly used as antimicrobial agents, photocatalysts (Abdelhakim et al. 2020), and biosensors (Aini et al. 2015). Currently, NPs are synthesized via different approaches (e.g., physical, chemical, and biological schemes). The physical and chemical methods use toxic chemicals, require high energy, and are difficult synthesis processes (Iravani et al. 2014). Therefore, biological methods (especially green synthesis) are preferable because of the use of diverse natural biological substances as the reducing and stabilizing agents (including yeast, fungi, bacteria, marine algae, and plant extracts) (Iravani et al. 2014). A wide range of bioactive reducing metabolites such as ketones, aldehydes, amides, and carboxylic acids have been associated with the reduction process of NPs, also known as green synthesis. Aqueous extract for green synthesis is safer than a chemical solvent, decreases waste and the pollution released into the environment (Owaid 2019). Numerous researchers have employed several plant species for this biological synthesis, including *Mentha pulegium* L. (Rad et al. 2019), *Cinnamomum camphora* (Aref & Salem 2020), *Diospyros malabarica* (Bharadwaj et al. 2021), *Thymbra spicata* L. (Gur et al. 2022), and *Mimusops elengi* Linn. (Prakash et al. 2013). The plant species *M. elengi* belongs to the Sapotaceae family and is widely distributed in tropical regions (i.e., India, Sri Lanka, the Andaman Islands, Myanmar, Indo-China, and northern Australia) (Baliga et al. 2011; Gami et al. 2012). It is also known as bullet wood (English), tanjung (Indonesian), bakul (Bengali), pikul (Thai), and enengi (Malaysian). The fruit, flowers, and bark of this plant are sweet and possess ethno-medicinal properties (e.g., antichronic dysentery, anticonstipation, diuretic effect, headache relief, and oral health care) (Baliga et al. 2011; Gami et al. 2012), and the leaves have been used for the treatment of stupor and coma. Several studies have reported that the *M. elengi* leaves contain multiple active phytoconstituent chemicals (i.e., alkaloids, phenolics, flavonoids, terpenoids, tannins, and glycosides) useful for pharmaceutical purposes (Kar et al. 2012). Recently, AgNPs from *M. elengi* leaf extract was successfully synthesized. The obtained AgNPs exhibited antibacterial activity against multidrug-resistant strains and were found to be very stable (Prakash et al. 2013). However, the metal nanoparticle (Ag and ZnO) synthesized using *M. elengi*, its antioxidant application, and its cell viability have not yet been reported. Therefore, this study aims to use *M. elengi* leaf extract for the synthesis of both AgNPs and ZnONPs. The following synthesis parameters that influence the formation of both metal and metal oxide NPs were applied. Ultraviolet–visible (UV–Vis) spectroscopy was used as a preliminary confirmation for the formation of the NPs. Fourier transform infrared spectroscopy (FTIR) analysis was used to identify the functional group of biomolecules responsible for reducing the Ag^+ and Zn^{2+} ions. The crystalline structure of the NPs was confirmed using X-ray diffraction (XRD). The morphology and particle size of the NPs were detected using transmission electron microscopy (TEM). Finally, the potential utilization of the AgNPs and ZnONPs for their antioxidant activity and cytotoxicity against colon cancer cells were evaluated.

Materials and Methods

Preparation of the *Mimusops elengi* leaf extract

The *M. elengi* leaves were collected from Pattani Province, Thailand. The leaves were shade dried and ground into a powder with a disc mill for 20 min. Next, 25 g of the dried powder was macerated with 125 mL of deionized water overnight at room temperature (RT) with stirring. After filtering through Whatman No.1 filter paper, the automatic rotary evaporator was used to evaporate the filtrate at 70 °C for 6 h to get the crude extract (Singleton et al. 1999).

TOTAL PHENOLIC CONTENT

The crude extract solution was mixed with distilled water and 10% Folin–Ciocalteu reagent. The mixture was incubated for 6 min at RT. Then, 7% Na_2CO_3 solution and distilled water were mixed and incubated for 15 min at 45 °C. The absorbance of the extract solution was determined at 765 nm. Gallic acid was used as a standard. The total phenolic content (TPC) was expressed as milligrams of gallic acid equivalents per gram of extract (mg GAE/g extract) (Singleton et al. 1999).

TOTAL FLAVONOID CONTENT

The extract solution and 5% $NaNO_2$ were mixed and incubated at RT for 5 min. Then, 120 µL of 10% $AlCl_3$ was added; this stood for 5 min for the reaction to occur. Next, 1-mM NaOH and distilled water were added to complete the reaction. The absorbance was determined at 510 nm. Catechin was used as a standard. The total flavonoid content (TFC) was expressed as milligrams of catechin equivalents per gram of extract (mg CE/g extract) (Singleton et al. 1999).

HIGH-PERFORMANCE LIQUID CHROMATOGRAPHY WITH DIODE-ARRAY DETECTION ANALYSIS

The phenolic compounds in *M. elengi* leaf extract were investigated using a high-performance liquid chromatography with diode-array detection (HPLC-DAD) system by comparing them with the phenolic compounds in standard mixtures. The HPLC-DAD apparatus (Agilent Technologies, CA, USA) equipped with Phenomenex ODS column (4.6 × 250 mm, 5 µm) monitored samples at different wavelengths: 254 nm for gallic and chlorogenic acids; 270 nm for ellagic acid; 280 nm for catechin and epicatechin; 340 nm for ferulic acid; and 370 nm for myricetin, quercetin, and kaempferol. The injection volume of the extract solution was 10 µL. The separation was carried out at RT with a C18 guard column. The mobile phase contained phosphoric acid and acetonitrile with a gradient ratio of the mobile phase (Moussi et al. 2015).

GREEN SYNTHESIS OF THE SILVER AND ZINC OXIDE NANOPARTICLES

For the AgNPs, 1 mL of the extract solution, at concentrations of 1,000-5,000 ppm, was dissolved in 10 mL of $AgNO_3$ solution at various concentrations (1-7 mM). To optimize the best conditions for the synthesis of the NPs, the solutions were incubated by stirring at 400 rpm at 25-70 °C and a pH of 3-11 for 30-120 min. After the solution changed to a reddish colour, it was evaporated at 70 °C for 1 h and heated by a hot air oven for 6 h at 90 °C until dark dried powder was obtained (Prakash et al. 2013). For the ZnONPs, 0.1-M zinc acetate dehydrate solution was mixed with 25 mL of the 1,000-ppm leaf extract solution using a magnetic stirrer for 120 min at 60 °C. Then, the reaction stood for 8 h. The particles were separated by centrifugation for 20 min at 6,000 rpm. The supernatant or concentrate extract was washed with distilled water followed by methanol. The precipitate was dried at 80 °C in a hot air oven. The crude calcination was carried out in a furnace at 350 °C for 3 h (Abdelhakim et al. 2020). Figure 1(A) presents the diagram for the green synthesis of the AgNPs and ZnONPs using *M. elengi* leaf extract.

INVESTIGATION OF NANOPARTICLE FORMATION USING ULTRAVIOLET–VISIBLE SPECTROPHOTOMETRY

This study utilized UV-Vis spectrophotometry to confirm the formation of the synthesized AgNPs and ZnONPs. This was done by recording the absorbance on a UV-Vis spectrophotometer (Biochrom, Cambridge, UK) in the range of 300-800 nm. The strong absorption in the visible region (420-500 nm) is called the surface plasmon resonance (SPR) phenomenon (Ramesh et al. 2018).

FUNCTIONAL GROUP ANALYSIS USING FOURIER TRANSFORM INFRARED SPECTROSCOPY

The FTIR spectra were recorded with frequencies ranging from 280 to 4,000 cm^{-1} for the *M. elengi* leaf extract, the AgNPs, and the ZnONPs in a KBr matrix using an FTIR spectrometer (Bruker, MA, USA) (Ramesh et al. 2018).

XRD ANALYSIS

The crystalline structure of the mono-phase compound was examined using XRD. Briefly, a thin film of the AgNPs or ZnONPs was prepared by coating the NP sample on carbon-coated Cu. The thin film of NPs was analyzed using an XRD goniometer (Mettler Toledo, OH, USA). Scanning was performed at 40 kV, 20 mA, using Cu-Kα/radiation (λ = 1.5418 Å) in the region of the 2θ angles ranging from 3 degree to 50 degree, with a scanning rate of 0.5 degree/min (Ramesh et al. 2018).

SIZE AND MORPHOLOGY ANALYSES USING TRANSMISSION ELECTRON MICROSCOPY

The morphology of the AgNPs and ZnONPs were

characterized using TEM (Jeol, Tokyo, Japan). The samples of NPs were prepared by dropping them on carbon-coated Cu grids and allowing them to dry at RT. The images were then captured at 40,000× magnifications with a voltage of 20.00 kV (Ramesh et al. 2018).

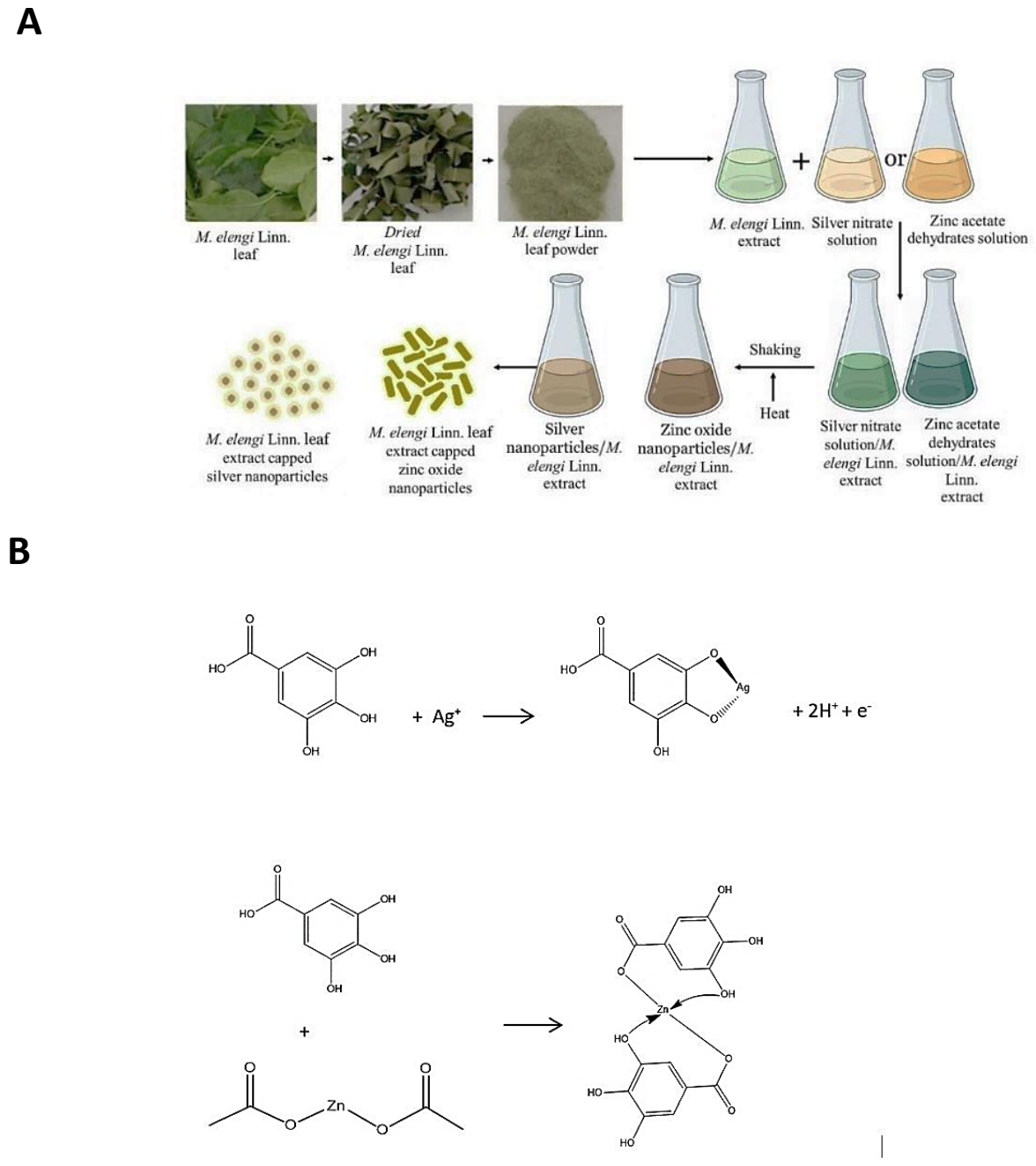

FIGURE 1. (A) The green synthesis of AgNPs and ZnONPs nanoparticles using *M. elengi* Linn. leaf extract (B) Synthesis mechanism of: AgNPs and ZnONPs

DPPH RADICAL SCAVENGING ASSAY

The 2,2-diphenyl-1-picrylhydrazyl (DPPH) scavenging activity was investigated to check the radical activity before and after green synthesis occurred. The Trolox standard or extract solutions, in different concentrations (7.8125-500 mg/L), were mixed with 0.2-mM DPPH dissolved in methanol and incubated at RT in the dark for 30 min. The absorbance was determined at 515 nm using a UV-Vis spectrophotometer (Singleton et al. 1999). The scavenging activity was calculated as follows:

$$\% \text{ Scavenging activity} = [1 - (Abs_{sample})/Abs_{blank}] \times 100 \quad (1)$$

The half maximal effective concentration (EC_{50}) was calculated from an equation that was obtained from a linear regression curve of the samples at various concentrations (Singleton et al. 1999).

ABTS RADICAL SCAVENGING ASSAY

The 2,2′-Azino-bis (3-ethyl benzothiazoline-6-sulfonic acid (ABTS) radical scavenging activity of the extract before and after the synthesis of the NPs was determined. The ABTS radical cation solution was prepared by mixing 7-mM ABTS solution with 4.9-mM Potassium persulfate solution. The mixture was incubated in the dark at 4 °C for 12-16 h before use. Samples having a concentration of 1,000 mg/L were mixed with 1 mL of the ABTS radical cation solution to study the scavenging activity. The reaction was allowed to develop at RT for 5 min. The absorbance was measured at a wavelength of 734 nm. Trolox was used as a standard solution to generate a standard curve. The percentage of ABTS radical cation scavenging was calculated using equation (1), and the EC_{50} was calculated as stated in the DPPH radical scavenging assay section (Singleton et al. 1999).

FERRIC REDUCING ANTIOXIDANT POWER ASSAY

The ferric reducing antioxidant power (FRAP) method was determined by preparing a FRAP reagent (300 mM acetate buffer, pH 3.6; 10 mM 2,4,6-Tris(2-pyridyl)-s-triazine (TPTZ) solution in 40 mM HCl; 20 mM $FeCl_3$ in a ratio of 10:1:1) that was incubated at 37 °C for 10 min. Then, 40 µL of the samples were mixed with 200 µL of distilled water and 1,200 µL of the FRAP reagent. The obtained blue solutions were kept at RT for 20 min. The absorbance was measured at a wavelength of 593 nm. The standard used was $FeSO_4$ (Benzie & Strain 1996).

CELL VIABILITY ASSAY

The Vero cell line (passage number 95-100) and Caco-2 cell line (passage number 55-60) (CLS Cell Lines Service GmbH, Eppelheim, Germany) were cultured in DMEM supplemented with 1% penicillin/streptomycin, 10% fetal bovine serum, and 2-mM stable L-glutamine. The cells were maintained in an atmosphere of 95% humidity and 5% CO_2 at 37 °C. All reagents for the cell cultures were obtained from Gibco, Life Technologies, Carlsbad, CA, USA. The cells (1×10^4 cells) were plated in a 96-well plate grown for 24 h in the incubator. The culture medium was removed and then replaced with the solutions of the extracts or the NPs diluted in culture medium ranging from 100 to 2,000 mg/mL. After the 24-h treatment, the culture medium was removed. Then, 200 µL of 0.5-mg/mL 3-(4,5-dimethylthiazol-2-yl)-2,5-diphenyltetrazolium bromide (MTT; Gibco, Life Technologies, Carlsbad, CA, USA) was added to each well and incubated for 4 h. The MTT solution was then removed. Next, 200 µL of dimethyl sulfoxide was added to each well to dissolve the formazan crystals metabolized from the viable cells. The violet solution was measured at 560 nm using a microplate reader and subtracted with the absorbance at 670 nm as the background (Wang et al. 2016). After the MTT assay, the cell viability was calculated using the following equation:

$$\text{Cell viability (\%)} = (Abs_{Sample}/Abs_{Control}) \times 100. \quad (2)$$

STATISTICAL ANALYSIS

The results obtained were calculated using a one-way ANOVA for the mean differences among the potential antioxidant values of the AgNPs and ZnONPs. An independent t-test was performed to analyze the differences between the extract (non-NP) and the NP treatment of the crude extracts. The statistical significance was examined at a level of $p < 0.05$.

RESULTS AND DISCUSSION

PHYTOCHEMICALS IN THE *Mimusops elengi* LEAF EXTRACT

It has been reported that the *M. elengi* aqueous extract is composed of various compounds that are responsible for both the reduction and stabilization of the NPs (Gami et al. 2012; Kar et al. 2012). In this study, the water extractive value (the yield) of the *M. elengi* leaf was 22.80±1.91% plant powder. The extract primarily contained highly polar compounds, especially phenolics and flavonoids. The total phenolic and flavonoid contents of the crude *M. elengi* leaf extract were 266.58±45.27 mg GAE/g extract and 151.13±3.77 mg

CE/g extract, respectively (shown in Table 1). Previous reports have indicated that phenolics and flavonoids are effective reducing agents, whereas proteins and some other phytochemicals are capping agents for AgNPs (Ravichandran et al. 2019). The enol of the phenolic and flavonoid compounds may release an electron by breaking the O–H bond; the released electron may be used to reduce the Ag^{+} to Ag^{0}. The HPLC-DAD determination was also conducted to identify the phenolic compounds in the crude *M. elengi* leaf extract. The peak obtained from the HPLC-DAD analysis was compared with the retention time of the phenolic standards. The results showed that the two main phenolic compounds found in *M. elengi* leaf extract, gallic, and ellagic acids, had retention times of 9.806 and 30.554 min, respectively. The results also indicated that gallic acid likely acts as the major phenolic compound in the extract and is facilitated as a reducing agent. On the basis of the TPC, TFC, and HPLC-DAD results, the phytochemicals present in the aqueous extract of *M. elengi* are the natural reducing agents responsible for the formation of the AgNPs and ZnONPs in green synthesis. The proteins and enzymes present in the leaf extract are likely responsible for the stability of the particles (Singh et al. 2018). The possible synthesis mechanisms of the AgNPs and ZnONPs, using the *M. elengi* leaf, are shown in Figure 1(B). The AgNPs can be formed when one of the –OH groups from the phenolic compound reacts with the Ag^{+} ion in the metal salt. The ZnONPs can be formed when two –OH groups from the phenolic compound react with the Zn^{2+} ion (Alamdari et al. 2020). However, further investigation on the green synthesis formation mechanism of the AgNPs and ZnONPs is necessary for a better understanding of the chemical processes and reactions that occur. The phenolic compounds present in the *M. elengi* leaf extract are shown in Table 2.

TABLE 1. Yield of extract, total phenolic and total flavonoid contents of *Mimusops elengi* Linn.

Phytochemical contents	Values
Yield of crude extract (%)	22.80 ± 1.91
Total phenolic content (mg GAE/g extract)	266.58 ± 45.27
Total flavonoid content (mg CE/g extract)	151.13 ± 3.77

GAE: Gallic acid equivalent; CE: Catechin equivalent
Data are expressed as mean ± SD from three-independent experiments

TABLE 2. Identification of individual phenolic and flavonoid compounds of *M. elengi* crude extract at 280 nm using HPLC-DAD system

Standard phenolic compounds	Retention time (min)	Maximum wavelength (nm)	Area (mAU)
myricetin	36.882	370	undetected
quercetin	43.018	370	undetected
kaempferol	48.923	370	undetected
gallic acid	9.806	254	527.2
chlorogenic acid	22.127	254	undetected
catechin	22.177	280	undetected
epicatechin	25.178	280	undetected
ellagic acid	30.554	270	53.9
ferulic acid	32.177	340	undetected

GREEN SYNTHESIS OF NANOPARTICLES

Several plant biomolecules play a major role in the bioreduction and stabilization of the green synthesis of metal NPs. The polyphenols and enzymes in the plants can affect the NP production due to the polyphenolics present in the leaves are likely to self-oxidize because of the oxidative enzymes and oxygen molecules (Marslin et al. 2018). The addition of the leaf extracts to a solution containing metal salts ($AgNO_3$ and $ZnC_4H_6O_4$) showed a colour change within 30 min. The colour changed from colourless to yellow-brown, indicating the excitation of the SPR and the reduction of the metal. However, when plant extracts were not added, no changes were noted in the $AgNO_3$ solution. The formation of the metal NPs can be simply observed using UV–Vis spectroscopy at the wavelength range of 400-470 nm. The SPR phenomenon principally occurred because of the interaction of the electromagnetic radiation and the electrons in the conduction band around the metal NPs (Ramesh et al. 2018). A sharper SPR peak suggests the formation of smaller and more uniform NPs, whereas a broader SPR peak indicates larger NPs. The $AgNO_3$ and leaf extract solutions were mixed and incubated by stirring at 400 rpm, 25-70 °C, with a pH of 11, for 90 min. The absorption peak at the wavelength of 423 nm indicated the formation of the AgNPs. The sharpest SPR peak of the AgNPs was observed after 10 mL of the 5,000-ppm *M. elengi* extract was added to 1 mL of 3-mM $AgNO_3$, suggesting small, spherical shapes (depicted in Figure 2(A)). A broad peak was observed at 370 nm for the ZnONPs, likely due to the larger size of the synthesized ZnONPs (shown in Figure 2(B)). At high temperatures (80-120 °C), the reactant was rapidly consumed, resulting in a large number of small-diameter AgNPs. The absorbance value increased gradually as the pH range increased from 3 to 11, suggesting that the rate of the formation of the AgNPs was higher in basic pH than in acidic pH. The formation of the AgNPs occurred rapidly in basic pH (11). This was clear upon visual observation and may be due to the ionization of the phenolic group present in the extract, which agrees with a previous study (Ramesh et al. 2018). Therefore, the synthesis using a 10:1 ratio of 3-mM $AgNO_3$ and 5,000-ppm *M. elengi* leaf extract at 70 °C in a basic medium (pH = 11) for 90 min was chosen as the optimal condition for the green synthesis of the AgNPs. Conversely, the green synthesis of the ZnONPs was a very straightforward process that occurred when a Zn salt, e.g., $Zn(NO_3)_2$ or $ZnC_4H_6O_4$), was added into a biological agent; after which the mixture was thermally treated. The concentration of the Zn salts, leaf extract, and reaction temperature were varied to determine the best formation conditions of the ZnONPs. As the concentration of the extracts and temperature increased, the formation of the ZnONPs also increased. Thus, the optimal conditions for the green synthesis of the ZnONPs were 0.2-M $Zn(CH_3COOH)_2$ and 1,000-ppm leaf extract at 70 °C (depicted in Figure 2(B)).

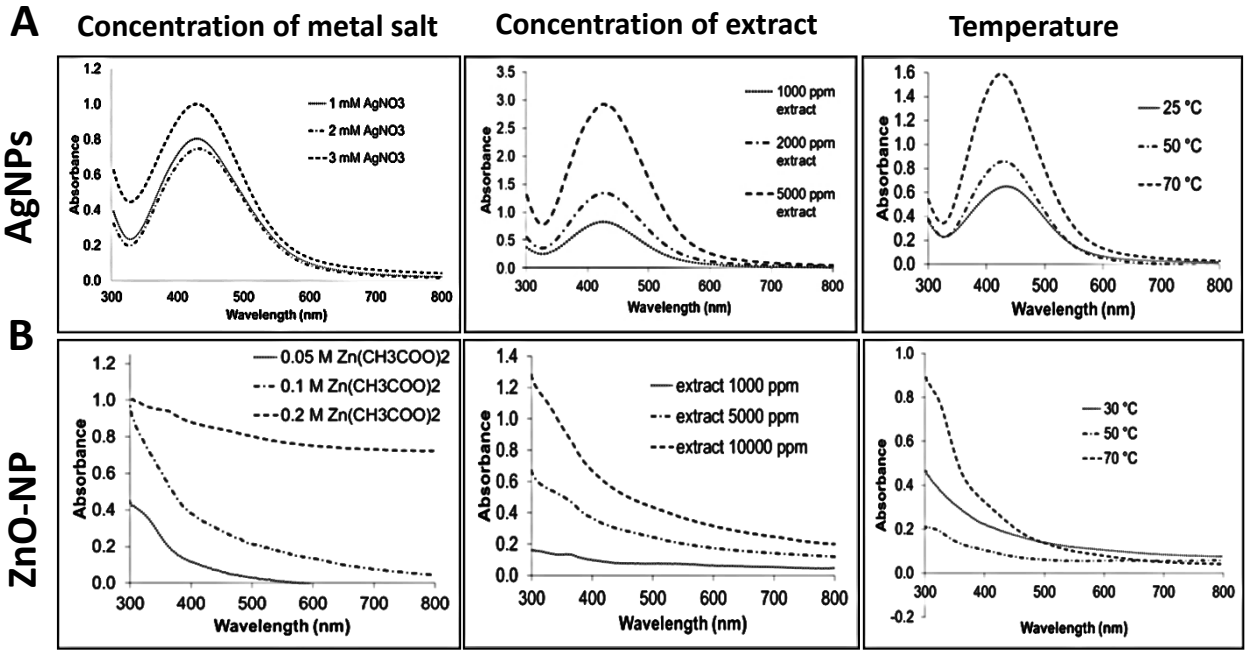

FIGURE 2. UV-Vis spectra of: (A) $AgNO_3$ prepared by different concentrations of metal salt silver nitrate ($AgNO_3$), concentration of *M. elengi* leaf extract and temperature of reaction, (B) ZnONPs prepared by different concentrations of metal salt or zinc acetate ($Zn(CH_3COO)_2$), concentration of *M. elengi* leaf extract and temperature of reaction

NANOPARTICLE CRYSTALLINE NATURE, SIZE, AND MORPHOLOGY

The crystalline nature of the AgNPs was confirmed using powder XRD. The XRD pattern of the AgNPs prepared using the *M. elengi* leaf extract is presented in Figure 3(A). The strong diffraction peaks at 2θ values were observed at 38.2, 44.5, 64.5, 77.5, and 81.5 °, corresponding to the (111), (200), (220), (311), and (222) interplanar reflections of a face-centered cubic (fcc) crystal structure. The intense reflection of the (111) peaks, compared with that of the other peaks, indicates that NPs were formed (Aref & Salem 2020). The XRD pattern of the ZnONPs is presented in Figure 3(B). The strong diffraction peaks at 2θ values were observed at 31.7, 34.4, 36.2, 47.5, 56.6, and 62.8°, corresponding to the (100), (002), (101), (102), (110), and (103) interplanar reflections of a hexagonal crystal structure, respectively. The intense reflection of the (101) peaks indicate that NPs were formed (Rad et al. 2019). The particle size and morphology of the AgNPs and ZnONPs were characterized using TEM results are shown in Figures 4(A) and 4(B). In Figure 4(A), the TEM results indicate that the AgNPs showed poly-dispersity and primarily spherical morphology with an average particle size of 22.12 nm; this is in the defined range for NP size (1-100 nm) (Khan et al. 2019). Figure 4(B) shows that the prepared ZnONPs had a rod-like shape (average particle size of 28.44 nm) and a thin-layered coat. This coat is possibly the organic substances in the *M. elengi* leaf extract that may be responsible for the stability of the NPs (Basnet et al. 2018).

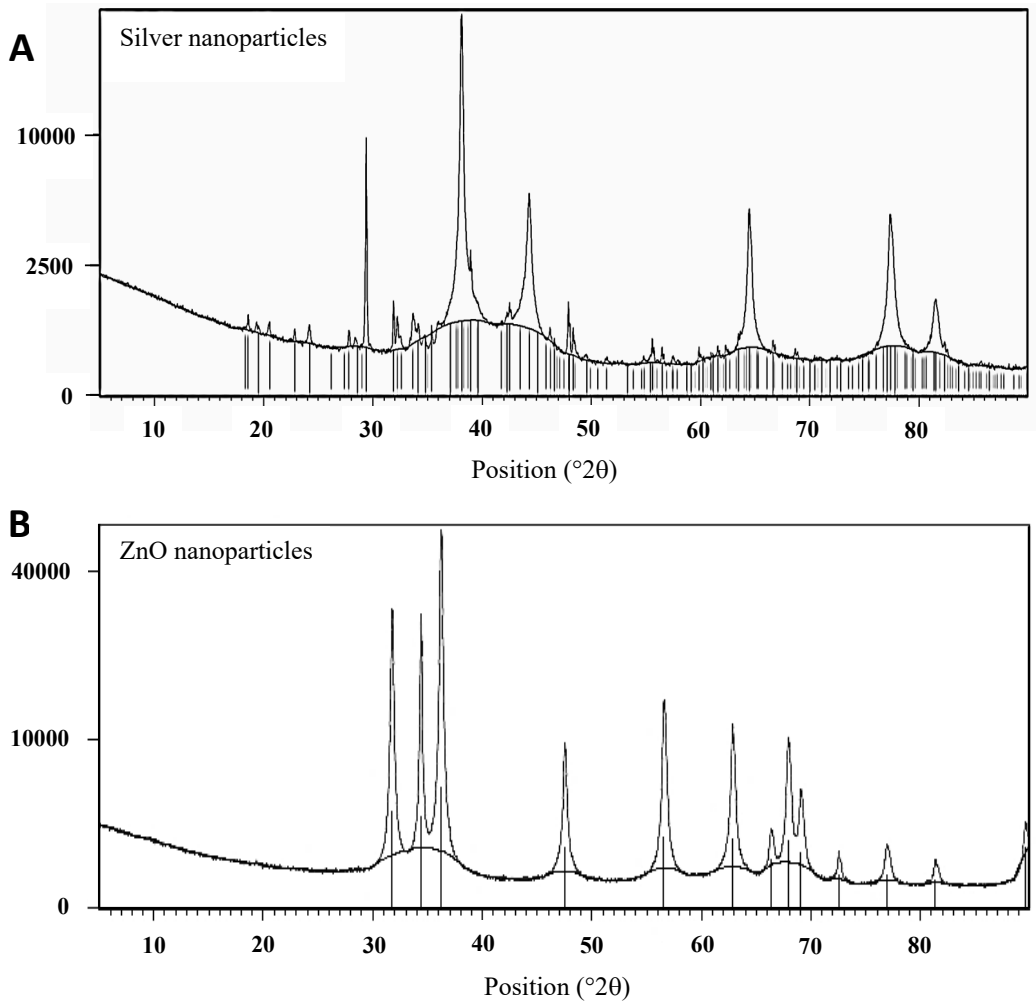

FIGURE 3. XRD analysis of (A) AgNPs, (B) ZnONPs

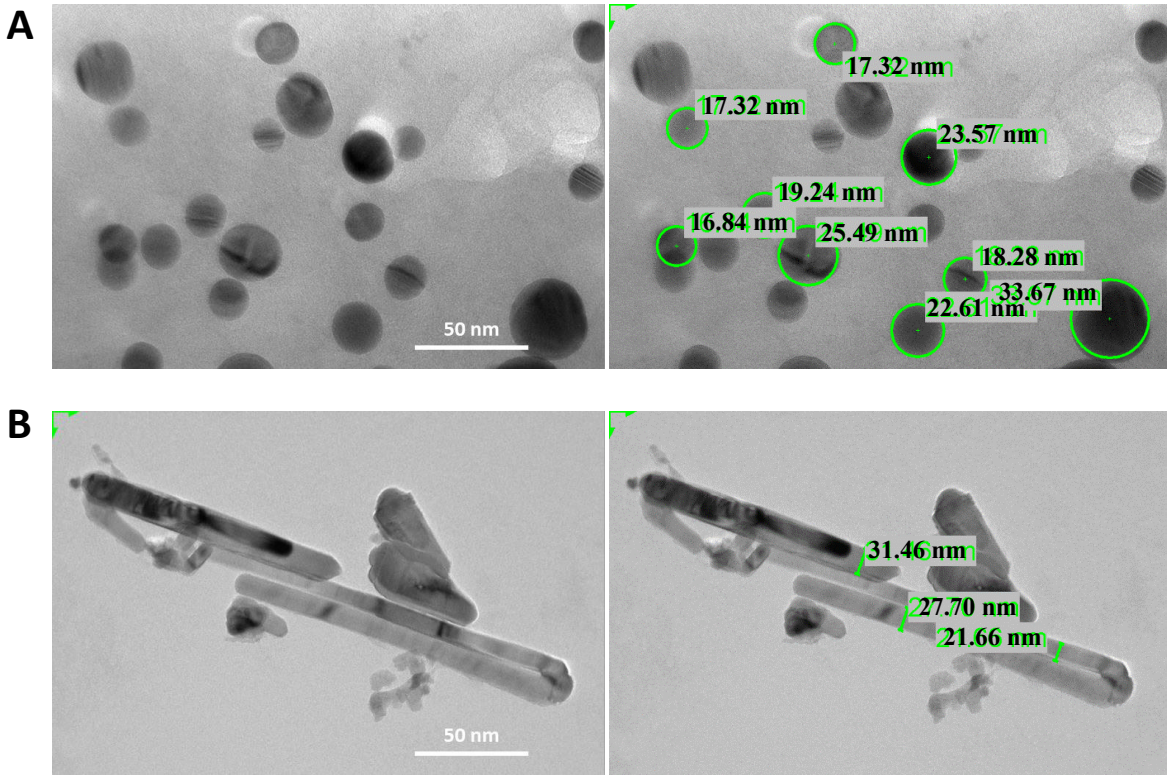

FIGURE 4. TEM images of: (A) AgNPs at 50 nm, (B) ZnONPs at 50 nm

DETERMINATION OF CAPPING AGENTS

It was assumed in a previous study that, in an extract, the phenolic compounds responded to the reduction process of the metal/metal oxide ions and that the protein molecules acted as capping and stabilizing agents (Singh et al. 2018). Therefore, this study's FTIR characterization aimed to determine the changing particle structure and functional groups of the samples before and after the synthesis. The FTIR spectra of the dried aqueous extract and synthesized AgNPs are shown in Figure 5(A). The band at 3,474 cm^{-1} corresponds to the O–H stretching of the H bonds of alcohol and phenol. The band at 2,426 cm^{-1} corresponds to the alkyne bond. The band at 1,641 cm^{-1} corresponds to the N–H bond of the primary amines. The band at 1,446 cm^{-1} corresponds to the C–O–H vibrations. The band at 1,383 cm^{-1} corresponds to the C–O stretching in the AgNPs. The band at 1,020 cm^{-1} corresponds to the C–O–C stretching. The FTIR results show clear evidence that both the–OH and $–NH_2$ groups are involved in both the green synthesis and capping of the AgNPs. The FTIR spectra of the ZnONPs are shown in Figure 5(B). The FTIR band at 3,425 cm^{-1} corresponds to the O–H stretching of the H bonds of alcohol and phenol. The band at 1,622 cm^{-1} corresponds to the N–H bond of the primary amines. The band at 1,385 cm^{-1} corresponds to the C–O stretching. The band at 1,023 cm^{-1} corresponds to the C–O–C stretching. The band at 541 cm^{-1} corresponds to the ZnO bond in the ZnONPs. The shift of the peaks from higher to lower signifies the formation of the ZnONPs. These results indicate that water-soluble compounds (i.e., polyphenols, flavonoids, alkaloids, and terpenoids) may play an important role as capping and reducing agents in the green synthesis of AgNPs and ZnONPs using *M. elengi* leaf extract. The obtained results are consistent with those of previous studies (Raja et al. 2017; Sharmila et al. 2019).

ANTIOXIDANT ACTIVITIES

Three different methods were used to determine the antioxidant activity potential of the *M. elengi* leaf extract, AgNPs, and ZnONPs. The DPPH and ABTS radical scavenging assays are relatively rapid and sensitive methods that evaluate the antioxidant activity

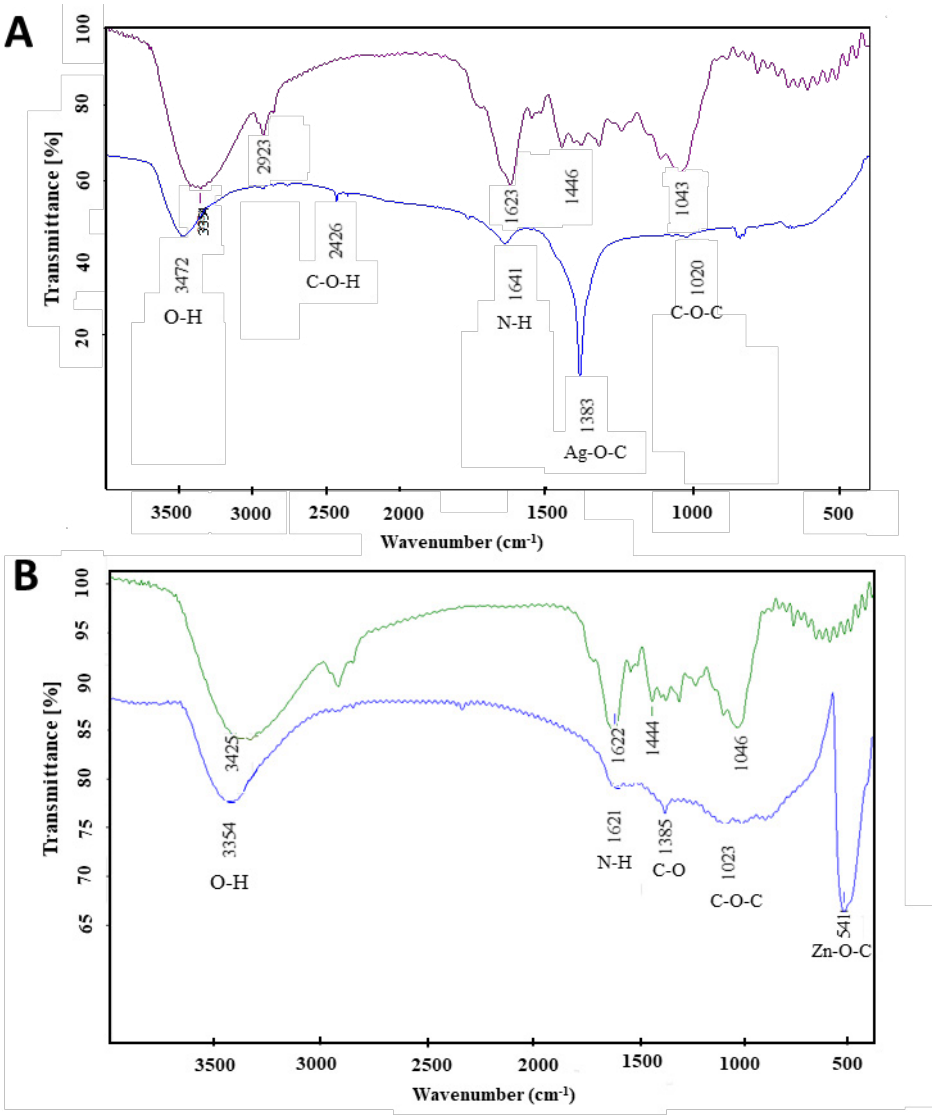

FIGURE 5. FTIR analysis of: (A) AgNPs, (B) ZnONPs

of compounds that react with free radical species. Meanwhile, the FRAP assay is the method utilized for determining the antioxidant activity via the ferro reduction of specific compounds or plant extracts. Trolox was used as a standard, and the antioxidant activity of the DPPH and ABTS assays were expressed as a Trolox equivalent antioxidant capacity (TEAC). The EC_{50} values of the *M. elengi* leaf extract, AgNPs, and ZnONPs were also obtained. Table 3 shows the TEAC and the EC_{50} values of the DPPH and ABTS assays as well as the ferro reduction equivalent value of the three samples (the *M. elengi* leaf extract, AgNPs, and ZnONPs). In both the DPPH and ABTS assay results, the TEAC decreased in the *M. elengi* leaf extract, AgNPs, and ZnONPs. The TEAC values were 433.52±2.50, 233.88±25.65, and 21.98±2.54 mg/g extract for the DPPH assay and 327.06±0.58, 197.63±16.76, and 24.74±0.24 mg/g extract for the ABTS assay. The EC_{50} value of the DPPH and ABTS assays tended to increase in the three samples. The obtained results demonstrate the effective antioxidant activity of the samples, and the *M. elengi* leaf extract's activity was higher than that of the AgNPs and ZnONPs. This was because no heat or chemical treatments were applied to the *M. elengi* leaf extract. However,

during the synthesis of the AgNPs and the ZnONPs, the antioxidant compounds could have decomposed. For the FRAP assay, the ferro reduction equivalent values of the *M. elengi* leaf extract, AgNPs, and ZnONPs were 4.03±0.23, 0.97±0.19, and 0.09±0.01 µM/mM extract, respectively. The phenolic compound found in the *M. elengi* leaves had a higher potential as an antioxidant and tended to decrease during the synthesis processes. The significant antioxidant potential of the AgNPs and ZnONPs is due to the hydrogen-donating ability of the compounds in the extract (e.g., the polyphenols) that capped the particles. The H^+ ion that capped the particles enabled the neutralization of the free radicals and prevented the oxidation that could reduce the cellular damages caused by oxidative stress (Kumar et al. 2014). Therefore, the phytochemicals in the *M. elengi* leaf extract can be considered a very good source of the substances responsible for the formation of the AgNPs and ZnONPs as well as for their antioxidant activities.

TABLE 3. Antioxidant activities of green synthesized Ag and ZnO nanoparticles

Compounds	DPPH		ABTS		FRAP (µM/mg)
	TEAC (mg/g)	EC_{50} (mg/L)	TEAC (mg/g)	EC_{50} (mg/L)	
Extract	433.52 ± 2.50	139.97 ± 25.16	327.06 ± 0.58	37.34 ± 4.38	4.03 ± 0.23
AgNPs	233.88 ± 25.65	237.33 ± 29.07	197.63 ± 16.76	215.45± 19.58	0.97 ± 0.19
ZnONPs	21.98 ± 2.54	5380.20 ± 420.87	24.74 ± 0.24	2785.41 ± 196.84	0.09 ± 0.01

EFFECTS OF *Mimusops elengi* CRUDE EXTRACT AND NANOPARTICLES ON CELL SURVIVAL

Utilizing medicinal plants to synthesize NPs is preferable because they are nontoxic and suitable for therapeutic use in medical sciences. The potential of nanotechnology can increase the efficiency of drug targeting and decrease drug toxicity. The cellular survival of normal and cancerous cells was investigated for its future possible biomedical applications. The effect of the crude extract and NPs on the survival of African green monkey kidney (Vero) cells and Caco-2 cells, the normal and cancerous cells, respectively, was examined using MTT assay. The cell viability was analyzed after the cells were treated with the tested compounds for 24 h. As shown in Figure 6, the crude extract concentrations of 125-2,000 µg/mL did not result in a cytotoxic effect on the Vero cells (Figure 6(A)), whereas a significant cytotoxicity was detected in the Caco-2 cells with a concentration of 2,000 µg/mL (Figure 6(A)). This result indicates that the crude extract exhibited anticancer activity. Ganesh et al. (2014), Kar et al. (2012), and Xu and Mao (2016) also studied the anticancer activity of *M. elengi* leaves in human cancer cell lines. The results of both studies indicated that the crude methanol extract of the *M. elengi* leaves exhibited cytotoxicity against Ehrlich's ascites carcinoma *in vitro* and *in vivo* (Ganesh et al. 2014; Xu & Mao 2016) and cervical cancer (SiHa) cells *in vitro* (Xu & Mao 2016). These studies indicated that the cytotoxicity may be due to the antioxidant properties and the cytotoxic compounds present in the crude extract (Kar et al. 2012). This study found that the crude water extract of the *M. elengi* leaves primarily contained gallic and ellagic acids, both of which have been recognized as antioxidant compounds possessing anticancer activity (Ceci et al. 2018; Wang et al. 2016). This study also assessed the effect of the AgNPs and ZnONPs on the survival of Vero and Caco-2 cells. As shown in Figure 6(B) and 6(C), the AgNPs and ZnONPs, at concentrations ranging from 7.8 to 125 µg/mL, did not have a cytotoxic effect on the cell lines. Furthermore, the NPs significantly increased the viability of the Vero cell line at 125 µg/mL. This result was contrary to several studies showing that metallic NPs possess cytotoxicity toward cancer cell lines (Poor et al. 2017). This is because the cytotoxicity of the metallic NPs depends on several factors: size, shape, solubility, coating surface and charges, tested concentration, time of exposure, and type

of cells (Zhang et al. 2016). Therefore, the size of the NPs may be a critical factor contributing to the differential cytotoxicity against the colon cancer cells. It has been suggested that small NPs (10 nm) are internalized in the cytoplasm more efficiently and demonstrate an increased toxicity compared with >20-nm NPs (Miethling-Graff et al. 2014). This suggestion was consistent with this study's observation because the sizes of the AgNPs and ZnONPs synthesized by the *M. elengi* extract were mostly >20 nm. The coating compounds of the NPs (e.g., sugars and glycosides) supply cell growth and were suggested to have a mild proliferative effect on the Vero cells (Ghramh et al. 2020). The ROS also plays a role here as signaling transduction and second messengers in cell stress responses and cellular physiology. The ROS can set multiple cancer-related signaling pathways by causing reversible oxidative post-translational modifications. A greater level of ROS is important for the viability of cancer cells because of the prolificacy of the cells and metastasis that occurs via redox signaling regulation (Xu & Mao 2016). As a result, the cell growth induction of the AgNPs and ZnONPs synthesized by the *M. elengi* extract in normal cells may provide some other therapeutic purpose, such as wound healing (Ahmed et al. 2017). For this study's results, the NPs did have cytotoxic effects via the generation of ROS. However, the smaller NPs should enter the cancerous cells via the nucleus and cause DNA breakage, ultimately leading to cell death (Chandra et al. 2020).

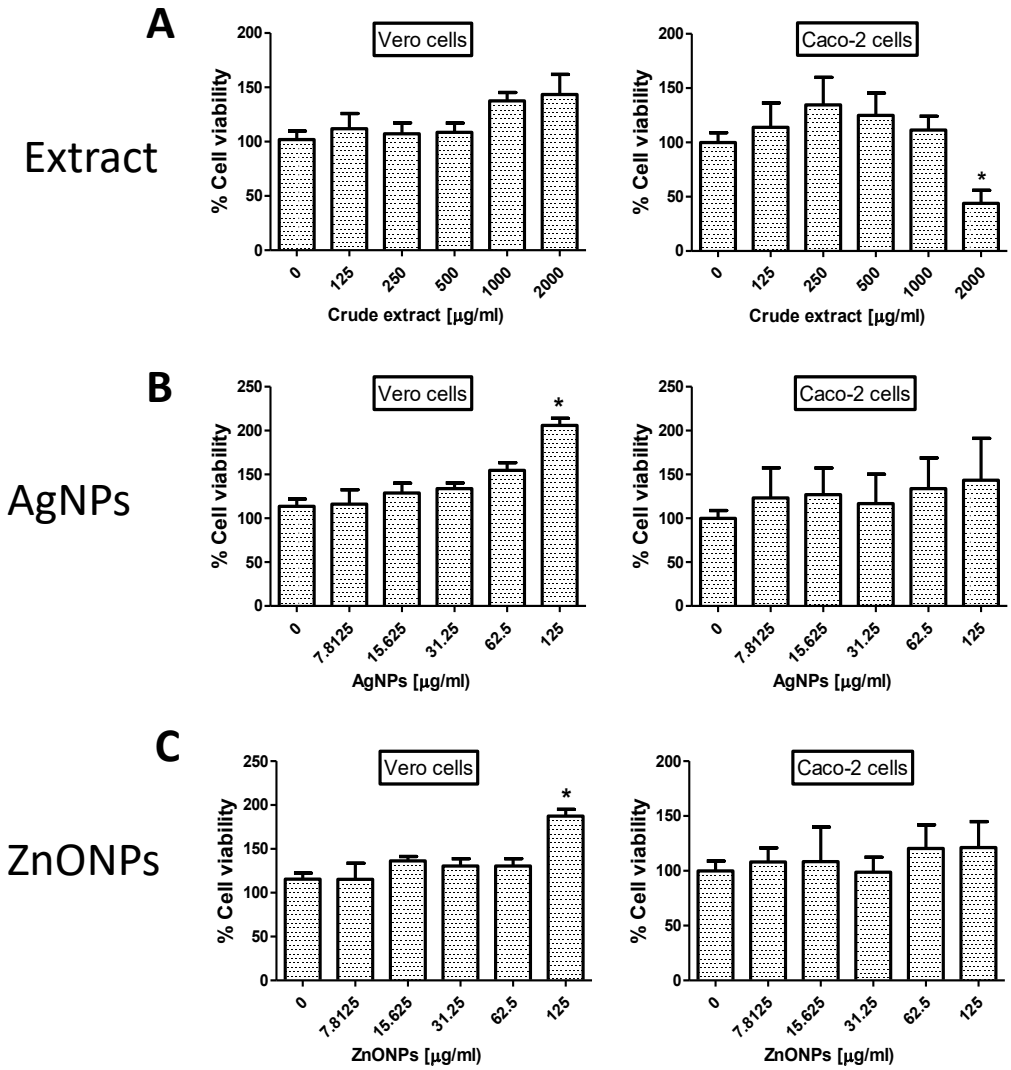

FIGURE 6. Cell viability of: (A) Vero and Caco-2 cell lines upon treatment with *M. elengi* leaf extract, (B) Vero and Caco-2 cell lines upon treatment with biosynthesized AgNPs, (C) Vero and Caco-2 cell lines upon treatment with biosynthesized ZnONPs at different concentrations for 24 h. % cell viability was displayed as mean ± SD from three independent experiment in triplicate. * p value < 0.05 versus control group without any treatment (µg/mL)

Conclusion

Both AgNPs and ZnONPs were synthesized using *M. elengi* leaf extract and evaluated for their antioxidant activity and cytotoxicity against colon cancer cells. The optimal conditions for the green synthesis of the AgNPs were 3-mM $AgNO_3$ with 1,000-ppm crude extract (10:1 ratio) at 70 °C in basic medium (pH = 11) for 90 min. The optimal conditions for the green synthesis of the ZnONPs were 0.2-M $Zn(CH_3COOH)_2$ with 5,000-ppm crude extract at 70 °C. The results of the SPR from the UV–Vis, FTIR, and TEM analyses showed that the AgNPs and ZnONPs were nano-sized with spherical and rod-like morphology, respectively. The size of the AgNPs obtained in this study ranged from 16.84 to 33.67 nm with fcc crystal structure, whereas the size of the ZnONPs ranged from 18.56 to 40.04 or 28.44 nm with hexagonal crystal structure. The AgNPs and ZnONPs exhibited good antioxidant activity in scavenging both DPPH and ABTS radicals. The EC_{50} values indicated that the AgNPs were more effective against the ABTS radicals (compared with the DPPH radicals) than the ZnONPs because of their higher sensitivity. The cytotoxicity test of the AgNPs and ZnONPs showed that they had no effect on the Caco-2 cells compared with the crude *M. elengi* extract but that they did have a cell growth effect on the Vero cells. Therefore, the metal NPs synthesized in this study may be utilized as efficient biomedical therapeutic agents. However, future studies are required for additional understanding of their action mechanisms before this recommendation can be made.

Acknowledgements

This study was supported by The *Scholarship* Awards for Master and Ph.D. Studies Thailand›s Education Hub for ASEAN Countries (*TEH-AC*) Scholarship and Thesis Research Grant from Graduate School of Prince of Songkla University. This study was also supported by the Applied Chemistry Research Program of the Department of Science, Faculty of Science and Technology, Prince of Songkla University, Pattani Campus, Thailand.

References

Abdelhakim, H.K., El-Sayed, E.R. & Rashidi, F.B. 2020. Biosynthesis of zinc oxide nanoparticles with antimicrobial, anticancer, antioxidant and photocatalytic activities by the endophytic *Alternaria tenuissima*. *Journal of Applied Microbiology* 128(6): 1634-1646.

Ahmed, B., Hashmi, A., Khan, M.S. & Musarrat, J. 2018. ROS mediated destruction of cell membrane, growth and biofilms of human bacterial pathogens by stable metallic AgNPs functionalized from bell pepper extract and quercetin. *Advanced Powder Technology* 29(7): 1601-1616.

Ahmed, S., Chaudhry, S.A. & Ikram, S. 2017. A review on biogenic synthesis of ZnO nanoparticles using plant extracts and microbes: A prospect towards green chemistry. *Journal of Photochemistry and Photobiology B: Biology* 166: 272-284.

Aini, B.N., Siddiquee, S., Ampon, K., Rodrigues, K.F. & Suryani, S. 2015. Development of glucose biosensor based on ZnO nanoparticles film and glucose oxidase-immobilized eggshell membrane. *Sensing and Bio-Sensing Research* 4: 46-56.

Alamdari, S., Ghamsari, M.S., Lee, C., Han, W., Park, H.H., Tafreshi, M.J., Afarideh, H. & Ara, M.H.M. 2020. Preparation and characterization of zinc oxide nanoparticles using leaf extract of *Sambucus ebulus*. *Applied Sciences* 10(10): 3620.

Aref, M.S. & Salem, S.S. 2020. Bio-callus synthesis of silver nanoparticles, characterization, and antibacterial activities via *Cinnamomum camphora* callus culture. *Biocatalysis and Agricultural Biotechnology* 27: 101689.

Baliga, M.S., Pai, R.J., Bhat, H.P., Palatty, P.L. & Boloor, R. 2011. Chemistry and medicinal properties of the Bakul (*Mimusops elengi* Linn): A review. *Food Research International* 44(7): 1823-1829.

Bandeira, M., Giovanela, M., Roesch-Ely, M., Devine, D.M. & Crespo, J.S. 2020. Green synthesis of zinc oxide nanoparticles: A review of the synthesis methodology and mechanism of formation. *Sustainable Chemistry and Pharmacy* 15: 100223.

Basnet, P., Chanu, T.I., Samanta, D. & Chatterjee, S. 2018. A review on bio-synthesized zinc oxide nanoparticles using plant extracts as reductants and stabilizing agents. *Journal of Photochemistry and Photobiology B: Biology* 183: 201-221.

Benzie, I.F. & Strain, J.J. 1996. The ferric reducing ability of plasma (FRAP) as a measure of "Antioxidant Power": the FRAP assay. *Analytical Biochemistry* 239(1): 70-76.

Bharadwaj, K.K., Rabha, B., Pati, S., Choudhury, B.K., Sarkar, T., Gogoi, S.K., Kakati, N., Baishya, D., Kari, Z.A. & Edinur, H.A. 2021. Green synthesis of silver nanoparticles using *Diospyros malabarica* fruit extract and assessments of their antimicrobial, anticancer and catalytic reduction of 4-nitrophenol (4-NP). *Nanomaterials* 11(8): 1999.

Ceci, C., Lacal, P.M., Tentori, L., De Martino, M.G., Miano, R. & Graziani, G. 2018. Experimental evidence of the antitumor, antimetastatic and antiangiogenic activity of ellagic acid. *Nutrients* 10(11): 1756.

Chandra, H., Kumari, P., Bontempi, E. & Yadav, S. 2020. Medicinal plants: Treasure trove for green synthesis of metallic nanoparticles and their biomedical applications. *Biocatalysis and Agricultural Biotechnology* 24: 101518.

Dubey, R.S., Rajesh, Y.B.R.D. & More, M.A. 2015. Synthesis and characterization of SiO_2 nanoparticles via sol-gel method for industrial applications. *Materials Today: Proceedings* 2(4-5): 3575-3579.

Gami, B., Pathak, S. & Parabia, M. 2012. Ethnobotanical, phytochemical and pharmacological review of *Mimusops elengi* Linn. *Asian Pacific Journal of Tropical Biomedicine* 2(9): 743-748.

Ganesh, G., Abhishek, T., Saurabh, M. & Sarada, N.C. 2014. Cytotoxic and apoptosis induction potential of *Mimusops elengi* L. in human cervical cancer (SiHa) cell line. *Journal of King Saud University - Science* 26(4): 333-337.

Ghramh, H.A., Ibrahim, E.H. & Kilany, M. 2020. Study of anticancer, antimicrobial, immunomodulatory, and silver nanoparticles production by Sidr honey from three different sources. *Food Science & Nutrition* 8(1): 445-455.

Gur, T., Meydan, I., Seckin, H., Bekmezci, M. & Sen, F. 2022. Green synthesis, characterization and bioactivity of biogenic zinc oxide nanoparticles. *Environmental Research* 204: 111897.

Iravani, S., Korbekandi, H., Mirmohammadi, S.V. & Zolfaghari, B. 2014. Synthesis of silver nanoparticles: Chemical, physical and biological methods. *Research in Pharmaceutical Sciences* 9(6): 385-406.

Istiqola, A. & Syafiuddin, A. 2020. A review of silver nanoparticles in food packaging technologies: Regulation, methods, properties, migration, and future challenges. *Journal of the Chinese Chemical Society* 67(11): 1942-1956.

Kar, B., Kumar, R.S., Bala, A., Dolai, N., Mazumder, U.K. & Haldar, P.K. 2012. Evaluation of antitumor activity of *Mimusops elengi* leaves on Ehrlich's ascites carcinoma-treated mice. *Journal of Dietary Supplements* 9(3): 166-177.

Khan, I., Saeed, K. & Khan, I. 219. Nanoparticles: Properties, applications and toxicities. *Arabian Journal of Chemistry* 12(7): 908-931.

Kokila, T., Ramesh, P.S. & Geetha, D. 2016. Biosynthesis of AgNPs using *Carica papaya* peel extract and evaluation of its antioxidant and antimicrobial activities. *Ecotoxicology and Environmental Safety* 134(2): 467-473.

Kumar, H.A.K., Mandal, B.K., Kumar, K.M., Maddinedi, S.B., Kumar, T.S., Madhiyazhagan, P. & Ghosh, A.R. 2014. Antimicrobial and antioxidant activities of *Mimusops elengi* seed extract mediated isotropic silver nanoparticles. *Spectrochimica Acta Part A: Molecular and Biomolecular Spectroscopy* 130: 13-18.

Marslin, G., Siram, K., Maqbool, Q., Selvakesavan, R.K., Kruszka, D., Kachlicki, P. & Franklin, G. 2018. Secondary metabolites in the green synthesis of metallic nanoparticles. *Materials* 11(6): 940.

Miethling-Graff, R., Rumpker, R., Richter, M., Verano-Braga, T., Kjeldsen, F., Brewer, J., Hoyland, J., Rubahn, H-G. & Erdmann, H. 2014. Exposure to silver nanoparticles induces size- and dose-dependent oxidative stress and cytotoxicity in human colon carcinoma cells. *Toxicology in Vitro* 28(7): 1280-1289.

Mondéjar-López, M., López-Jiménez, A.J., Abad-Jordá, M., Rubio-Moraga, A., Ahrazem, O., Gómez-Gómez, L. & Niza, E. 2021. Biogenic silver nanoparticles from *Iris tuberosa* as potential preservative in cosmetic products. *Molecules* 26(15): 4696.

Moussi, K., Nayak, B., Perkins, L.B., Dahmoune, F., Madani, K. & Chibane, M. 2015. HPLC-DAD profile of phenolic compounds and antioxidant activity of leaves extract of *Rhamnus alaternus* L. *Industrial Crops and Products* 74: 858-866.

Owaid, M.N. 2019. Green synthesis of silver nanoparticles by *Pleurotus* (oyster mushroom) and their bioactivity: Review. *Environmental Nanotechnology, Monitoring & Management* 12: 100256.

Paladini, F. & Pollini, M. 2019. Antimicrobial silver nanoparticles for wound healing application: Progress and future trends. *Materials* 12(16): 2540.

Poor, M.H.S., Khatami, M., Azizi, H. & Abazari, Y. 2017. Cytotoxic activity of biosynthesized Ag nanoparticles by *Plantago major* towards a human breast cancer cell line. *Rendiconti Lincei-Scienze Fisiche E Naturali* 28(4): 693-699.

Prakash, P., Gnanaprakasam, P., Emmanuel, R., Arokiyaraj, S. & Saravanan, M. 2013. Green synthesis of silver nanoparticles from leaf extract of *Mimusops elengi*, Linn. for enhanced antibacterial activity against multi drug resistant clinical isolates. *Colloids and Surfaces B: Biointerfaces* 108: 255-259.

Rad, S.S., Sani, A.M. & Mohseni, S. 2019. Biosynthesis, characterization and antimicrobial activities of zinc oxide nanoparticles from leaf extract of *Mentha pulegium* (L.). *Microbial Pathogenesis* 131: 239-245.

Raja, S., Ramesh, V. & Thivaharan, V. 2017. Green biosynthesis of silver nanoparticles using *Calliandra haematocephala* leaf extract, their antibacterial activity and hydrogen peroxide sensing capability. *Arabian Journal of Chemistry* 10(2): 253-261.

Ramesh, A.V., Devi, D.R., Battu, G. & Basavaiah, K. 2018. A facile plant mediated synthesis of silver nanoparticles using an aqueous leaf extract of *Ficus hispida* Linn. f. for catalytic, antioxidant and antibacterial applications. *South African Journal of Chemical Engineering* 26: 25-34.

Ravichandran, V., Vasanthi, S., Shalini, S., Shah, S.A.A., Tripathy, M. & Paliwal, N. 2019. Green synthesis, characterization, antibacterial, antioxidant and photocatalytic activity of *Parkia speciosa* leaves extract mediated silver nanoparticles. *Results in Physics* 15: 102565.

Sharmila, G., Thirumarimurugan, M. & Muthukumaran, C. 2019. Green synthesis of ZnO nanoparticles using *Tecoma castanifolia* leaf extract: Characterization and evaluation of its antioxidant, bactericidal and anticancer activities. *Microchemical Journal* 145: 578-587.

Singh, J., Dutta, T., Kim, K.H., Rawat, M., Samddar, P. & Kumar, P. 2018. Green synthesis of metals and their oxide nanoparticles: Applications for environmental remediation. *Journal of Nanobiotechnology* 16(84): 1-24.

Singleton, V.L., Orthofer, R. & Lamuela-Raventós, R.M. 1999. Analysis of total phenols and other oxidation substrates and antioxidants by means of Folin-Ciocalteu reagent. *Methods in Enzymology* 299: 152-178.

Wang, R., Ma, L., Weng, D., Yao, J., Liu, X. & Jin, F. 2016. Gallic acid induces apoptosis and enhances the anticancer effects of cisplatin in human small cell lung cancer H446 cell line via the ROS-dependent mitochondrial apoptotic pathway. *Oncology Reports* 35(5): 3075-3083.

Xu, J. & Mao, W. 2016. Overview of research and development for anticancer drugs. *Journal of Cancer Therapy* 7(10): 762-772.

Zhang, X.F., Shen, W. & Gurunathan, S. 2016. Silver nanoparticle-mediated cellular responses in various cell lines: An *in vitro* model. *International Journal of Molecular Sciences* 17(10): 1603.

*Corresponding author; email: weeraya.k@psu.ac.th